Mineralization of organic matter in microbialites and implications for microbialite reservoirs in Member IV of the Leikoupo Formation, Sichuan Basin, China

Yuan Zhong[1], Kunyu Li[1], Zili Zhang[1], Yanping Qiao[1], Guiping Su[1], Like Zhao[1], Baoshou Zhang[1], Yunlong Wang[1], Shuang Dou[1], Wei Yan[1] and Jie You[2]*

[1]Exploration and Development Research Institute, PetroChina Southwest Oil and Gasfield Company, Chengdu, China, [2]Sichuan Natural Gas Geology Key Laboratory, Southwest Petroleum University, Chengdu, China

Microbialites are important reservoirs for oil and gas. The mineralization of organic matter in microbialites during early diagenesis can produce acidic fluids that dissolve carbonate grains, and can also result in an alkaline pore water that precipitates cement. The mineralization of organic matter in microbialites and its effect on microbialite reservoirs have not yet been studied in detail. In this study, quantitative statistical analysis of the two-dimensional spatial occurrence of pores and microbial fabrics, *in situ* geochemical analysis of specific components (microbial, transitional zone, and fine spar fabrics), and qualitative evaluation of the implications for microbialite reservoirs were undertaken on microbialites from Member IV of the Leikoupo Formation, Sichuan Basin, China. The quantitative statistical analysis shows that pores are spatially associated with microbial fabrics, but porosity has a poor correlation with microbial fabric content. *In situ* geochemical data indicate that microbialites with different porosities experienced different processes of organic matter mineralization. The processes of organic matter mineralization such as oxidation and nitrate reduction can provide more dissolution micropores than the process related with sulfate reduction, whereas the process of organic matter mineralization related with Fe−Mn oxide reduction results in cementation. Micropores created by organic matter mineralization can act as fluid channels for later dissolution and are important in the development of microbialite reservoirs.

KEYWORDS

carbonate diagenesis, microbialite reservoir, *in situ* geochemistry, member IV, leikoupo formation, Sichuan basin

1 Introduction

Microbial carbonates (i.e., microbialites) are important oil and gas reservoirs, and a focus of recent research (e.g., Mancini et al., 2013; Rezende et al., 2013; Song et al., 2014; Chen et al., 2017). Many microbialite reservoirs are petroliferous, such as the Leikoupo Formation in the western Sichuan Basin (Wang, 2018; Wang et al., 2018; Zhao, 2020) and the Dengying Formation in the Sichuan Basin (Zou et al., 2014). Microbialites are deposited mainly in wide range of environments (Harwood and Sumner, 2011). Those microbialites in tidal environments are likely to be dissolved by meteoric water when relative sea level falls (Li

et al., 2015; Rezende and Pope, 2015; Song et al., 2017). However, good microbialite reservoirs are not always developed below karst surfaces, such as the Dengying Formation in the southern Sichuan Basin. It can be proposed that the development of microbialite reservoirs is not only related to secondary dissolution, but also to whether there were pre-existing channels for fluid to migrate and amplify reservoir space (Rezende and Pope, 2015).

Microbialites are formed through microbially induced mineral precipitation, grain trapping, and binding (Riding, 2000). The organic matter content in modern microbialites is generally high (Decho et al., 2015). Most organic material is degraded and consumed gradually during early diagenesis (i.e., through the mineralization of organic matter; Glunk et al., 2011). Previous studies have proposed that organic matter mineralization in microbialtes during early diagenesis can produce acidic fluids that dissolve carbonate minerals, but can also result in an alkaline pore water environment that precipitates carbonate cement (Visscher and Stolz, 2005; Dupraz et al., 2009). Micropores created by dissolution during organic matter mineralization can provide channels for subsequent meteoric fluids to accelerate karstification, enlarge pore sizes, and increase reservoir space. Cementation caused by organic matter mineralization will block pores, slow karstification, and decrease reservoir space.

Studies on the diagenesis of young sediments have shown that organic matter mineralization involves a series of complex biochemical processes (Canfield, 1991; Ingalls et al., 2004; Raiswell and Fisher, 2004), such as aerobic respiration, nitrate reduction, Fe–Mn oxide reduction, and sulfate reduction in order of decreasing Gibbs free energy (Forelich et al., 1979; Madigan et al., 1997; Widdicombe et al., 2011). Aerobic respiration and nitrate reduction lead to the dissolution of carbonate minerals, whereas Fe–Mn oxide reduction and sulfate reduction result in carbonate cementation (Visscher and Stolz, 2005). Therefore, it can be expected that different processes of organic matter mineralization will have variable impacts on the development of microbialite reservoirs, and these effects have not yet been studied in detail.

Microbialites from Member IV of the Leikoupo Formation in the Sichuan Basin, China, are good hydrocarbon reservoirs and have various microbial structures and pore types (Wu et al., 2011; Liu et al., 2016). The giant Pengzhou gas field, which has been recently discovered, has a daily well production of 42.4 MMCF (1.2 million m^3) of gas in the uppermost fourth member of the Middle Triassic Leikoupo Formation ($T_2l_4^3$) (Li et al., 2016). Therefore, Member IV of the Leikoupo Formation in the Pengzhou gas field provides ideal material for studying how organic matter mineralization affects the development of microbialite reservoirs. In this study, two common types of microbialite dolostone (stromatolite and thrombolite) and grain dolostone with different porosities in Member IV of the Leikoupo Formation were investigated. Quantitative statistical analysis of the two-dimensional spatial occurrence of pores and microbial fabrics, *in situ* geochemical analysis of specific components (microbial, transitional zone, and fine spar fabrics), and qualitative evaluation of the impacts of organic matter mineralization on the development of the microbialite reservoirs were conducted. The results provide new constraints on organic matter mineralization and its implications for microbialite reservoir development.

2 Geological setting

The Sichuan Basin is a subunit of the Yangtze paraplatform in southwestern China, which extends over an area of ~180,000 km^2. It is tectonically bounded by the Longmenshan fold belt to the northwest, the Micangshan uplift to the north, the Dabashan fold belt to the northeast, the Hubei–Hunan–Guizhou fold belt to the southeast, and the Emeishan–Liangshan fold belt to the southwest (Guo et al., 2004). During deposition of the Middle Triassic Leikoupo Formation, deep-seated, strike-slip faults were formed, and the central basin was uplifted and basin margin areas subsided (Regional Geology of Sichuan Province, 1988; Li et al., 2014). At this time, an arid climate existed, the Sichuan Basin transitioned into a restricted to evaporitic platform (Li et al., 2014). The YaS1 and Ys1 wells considered in this study are located in the giant Pengzhou gas field in the western Sichuan Basin (Supplementary Figure S1F).

The Middle Triassic Leikoupo Formation was deposited mainly in a restricted carbonate platform, including lagoonal, tidal, platform-edge shoal, and inner platform shoal settings (Ding et al., 2013; Peng et al., 2014). The Leikoupo Formation conformably overlies the Lower Triassic Jialingjiang Formation and is unconformably overlain by the Upper Triassic Xujiahe sandstone.

The Leikoupo Formation in the study area can be divided into four members (I–IV) from base to top (Regional Geology of Sichuan Province, 1988; Huang et al., 2011). Member I consists mainly of muddy dolostone, dolostone, and interbeds of dolomitic gypsum; Member II comprises gypsum and muddy dolostone or muddy limestone; Member III is mainly grain dolostone and dolostone; and Member IV comprises interbeds of dolostone and gypsum (Liu et al., 2016). Microbialites in the Leikoupo Formation are typically developed in Member IV, which have been termed "cryptalgal carbonates" (Liu, 1983), and classified into stromatolites, thrombolites, oncolites, and cryptalgal laminates (Liu et al., 2016). Microbialites in the Leikoupo Formation are all contemporaneous and penecontemporaneous dolomites (Liu, 1983; Liu et al., 2016). After deposition of the Leikoupo Formation in the Middle Triassic, the western Sichuan Basin was generally uplifted and exposed, and subjected to weathering, erosion, and karstification (Song et al., 2013; Tang, 2013; Liu et al., 2016).

3 Samples and methods

A total of 30 microbialite dolostone and grain dolostone samples with varying porosities were collected from Member IV of the Leikoupo Formation in wells YaS1 and Ys1 (Supplementary Figure S2). The grain dolostones were formed in association with the microbialites, and are also good reservoirs in the giant Pengzhou gas field.

Petrological investigations involved characterizing the morphology, structure, size, and occurrence of microbial fabrics and pores with a Leica 450C polarizing microscope. Microbial fabric and pore data (size and occurrence) were plotted on rose diagrams to examine the relationship between microbial fabrics and pores on thin sections. We orientated the extension of laminar films in stromatolites sample to east-west direction which is paralleling to bedding. However, the orientation of thrombolite sample is random.

Based on petrographic observations, three typical samples with different porosities (i.e., YaS-28, YaS-1, and YS-12) were selected for further detailed study. *In situ* geochemical profiles of specific components from the microbial fabric, transition zone, and fine spar fabric in these three samples were obtained to characterize

organic matter mineralization. The three specific components were identified from the size of the carbonate minerals and fabric features (Supplementary Figure S3F). The microbial fabric is a dark, dense micrite. Fine spar fabrics analyzed in this study have a crystal size of <30 μm. In the multi-stage cements, the *in situ* geochemical analyses were conducted on the finely crystalline isopachous dolomite cements that were identified as phase I cements by Wang et al. (2018). The transition zone is the area between the microbial and fine spar fabrics (Supplementary Figure S3).

In situ geochemical analyses were conducted with an Agilent 7700e inductively coupled plasma–mass spectrometer (ICP–MS) coupled to a GeolasPro laser ablation (LA) system. Detailed operating conditions of the LA–ICP–MS and data processing are described by Zong et al. (2017). The laser spot size and frequency were set to 44 μm and 5 Hz, respectively. Element concentrations were calibrated to reference materials (USGS carbonate pellet MACS-3 and basalt standards BHVO-2G, BCR-2G, and BIR-1G) without using an internal standard (Liu et al., 2008). Each analysis involved background acquisition for 20–30 s, followed by 50 s of data acquisition from the sample during ablation. Excel-based software ICPMSDataCal was used to perform off-line data selection, integration of background and analytic signals, drift corrections, and quantitative calibrations (Liu et al., 2008).

The petrology study was conducted at Southwest Petroleum University, Division of Key Laboratory of Carbonate Reservoir, CNPC, Chengdu, China. LA–ICP–MS analyses were undertaken at Wuhan Sample Solution Analytical Technology, Wuhan, China.

4 Results

4.1 Lithological and pore characteristics

4.1.1 Lithology

(1) Thrombolites: The thrombolites are represented by Sample YaS-1, and are developed near the base and in the upper part of Member IV of the Leikoupo Formation (Supplementary Figure S2). The thrombolites contain clots (Supplementary Figure S4A) that consist of dark grey to black micrites, have an irregular morphology, and range in size from 0.2 to 2 mm (Supplementary Figures S4B, C). There are many dissolution pores between the micro-scale clots, and these pores are always filled with thin fibrous and bladed dolomite cement.

In general, the thrombolites consist of micritic dolomite and loosely packed micro-scale clots (Supplementary Figure S4C). In addition, the absence of typical subaerial sedimentary structures (e.g., mud chips and fenestrae) suggests a subtidal setting for deposition of the thrombolitic microbialites.

(2) Stromatolites: The stromatolites are represented by Sample YS-12, and are developed mainly in the middle part and base of Member IV of the Leikoupo Formation (Supplementary Figure S2). The stromatolites comprise alternating slightly wavy dark and light layers (Supplementary Figure S4D, Figure 1A). The darker layers are micritic dolomites, whereas the light layers are mainly fine spar dolomites (Supplementary Figure S4C). The laminations in the stromatolites are laterally continuous and have a constant thickness of ~0.2 mm.

The slightly wavy layers and fine grain size (i.e., generally micrite) suggest that the stromatolites were deposited in a low-energy environment (Supplementary Figure S4E). Furthermore, the development of fenestral pores in the stromatolites (Supplementary Figure S4F) implies deposition in an upper intertidal or supratidal setting.
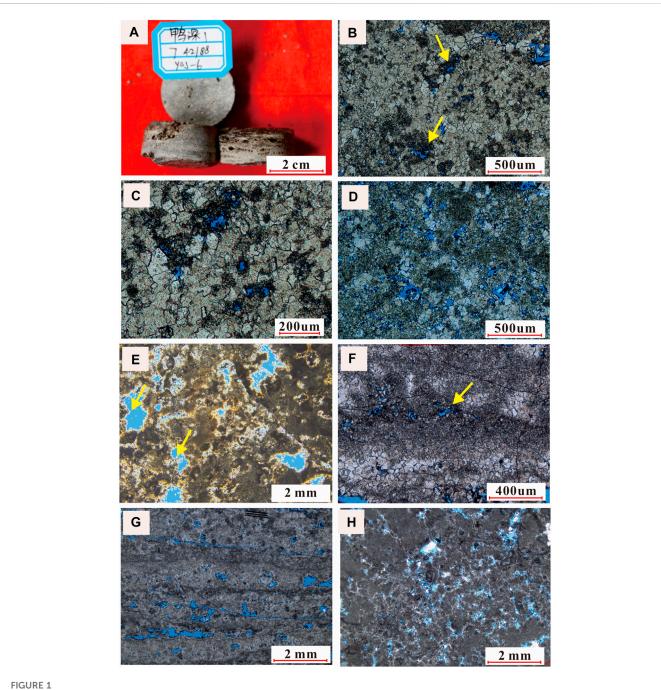
(3) Grain dolostones: The grain dolostones are represented by Sample YaS-28, and are found in the lower and upper parts of Member IV of the Leikoupo Formation (Supplementary Figure S2). Many loosely packed grains, composed of micrite, are visible under the microscope (Supplementary Figure S4H). The poorly sorted grains are moderately rounded, spherical or ellipsoidal, and range in size from 0.2–0.5 mm. The inter-granular space contains micritic and sparry dolomitic cement (Supplementary Figure S4I).

The large grain size of the grains suggests that the grain dolostones were deposited in a higher-energy setting than the thrombolites and stromatolites. The grain dolostones are often associated with the thrombolites and stromatolites, and form a common lithofacies association of thrombolites, grain dolostones, and stromatolites in ascending order (Supplementary Figure S2). Therefore, the grain dolostones are inferred to have been deposited between the lower intertidal and upper subtidal settings.

4.1.2 Pore characteristics

There are various pore classification schemes for microbialite reservoirs (Liu et al., 2016; Wang et al., 2017). To investigate the spatial relationship between microbial fabrics and pores, the pores in the microbialites were classified into five types based on the relative spatial occurrence of pores to microbial components and fabrics. These types comprise intra-clot, inter-clot, intra-microbial laminae, inter-microbial laminae, and inter-granular dissolution pores.

(1) Intra-clot dissolution pores: This type of pore is not well developed in the thrombolites. Intra-clot dissolution pores are isolated and have small sizes, usually ranging from 0.03 to 0.2 mm (Figures 1B, C). Some intra-clot dissolution pores are partially cemented by microcrystalline dolomites (Supplementary Figure S4B).

(2) Inter-clot dissolution pores: These pores are relatively abundant in the studied samples, and present mainly in the thrombolites. Inter-clot dissolution pores have good connectivity and vary in size from 0.2–1.0 mm (Figures 1D, E).

(3) Intra-microbial laminae dissolution pores: These pores are mainly developed in the stromatolites. Intra-microbial laminae dissolution pores are developed in the darker laminations, have their long axes parallel to the laminations, and are <0.1 mm in size (Figure 1F).

(4) Inter-microbial laminae dissolution pores: These pores are mainly present in the stromatolites, are more common than intra-microbial laminae dissolution pores, and are typically large (0.2–2.0 mm). The inter-microbial laminae dissolution pores occur between the darker laminations, and also have their long axes parallel to the laminations (Figures 1A, G).

(5) Inter-granular dissolution pores: These pores are most common in the grain dolostones, are well connected, and have large sizes of 0.5–1.0 mm (Figure 1H).

FIGURE 1
Pores charachteristics of microbialites in Member IV of the Leikoupo Formation. **(A)** Vuggys developed along the laminations in stramatolites; **(B,C)** The intra-clots dissolution pores with poor connectivity; **(D,E)** Inter-clots dissolution pores with a good connectivity; **(F)** Small intra-lamina dissolution pores; **(G)** Inter-lamina dissolution pores; **(H)** Inter-granular dissolution pores.

4.2 Geochemistry of the microbialite components

Trace elements can be used to track organic matter mineralization and carbonate diagenesis (Banner, 1995; Webb and Kamber, 2004; 2011). In particular, the elements Ce, Cr, Fe, Mo, and Cu are closely related to the process of organic matter mineralization (Shaw et al., 1990; Piper, 1994; Zheng et al., 2000; Algeo and Maynard, 2004).

The LA–ICP–MS data are listed in Table 1. In general, the concentrations of Cr, Mo, and Cu are low and show limited variation, with concentrations of 0.31–1.73 ppm (average = 1.16 ppm), 0.41–6.16 ppm (average = 2.86 ppm), and 0.04–0.93 ppm (average = 0.36 ppm), respectively. However, Fe concentrations in all samples have significant variations. Sample YS-12 has the highest Fe concentration of 217–521 ppm, whereas Sample YaS-1 has the lowest Fe concentration of 75.1–97.1 ppm.

Trace element concentrations of specific components (i.e., microbial, transitional, and fine spar fabrics) vary in the different samples (Table 1; Figure 2). In Sample YaS-1 (thrombolite), the lowest Cr concentration was observed in the

TABLE 1 Trace and major elements concentrations (ppm) of specific components.

Samples	YaS-1 (thrombolite)			YS-12 (Stromatolite)			YaS-28 (Grain dolostone)		
	YaS-1-01	YaS-1-02	YaS-1-03	YS-12-01	YS-12-02	YS-12-03	YaS-28-01	YaS-28-02	YaS-28-03
	Microbial fabric	Transitional zone fabric	Fine spar fabric	Microbial fabric	Transitional zone fabric	Fine spar fabric	Microbial fabric	Transitional zone fabric	Fine spar fabric
$MgCO_3$ (wt%)	57.3	57.5	55.9	58.0	57.9	58.3	63.2	94.9	76.7
$CaCO_3$ (wt%)	41.8	42.1	43.9	39.7	39.9	39.9	35.9	4.98	23.2
Sr	78.28	63.90	58.07	213.51	120.80	119.90	216.56	144.21	111.09
Na	176.03	177.71	193.15	394.35	349.61	283.37	141.24	56.79	101.86
Mn	12.72	13.58	10.53	19.64	18.32	20.10	12.23	6.77	8.92
Ba	1.34	1.33	0.96	20.57	3.82	4.65	6.37	1.66	14.68
Zn	0.28	0.24	0.07	0.76	0.61	0.60	0.79	0.06	0.01
Al	96.54	65.99	57.21	839.52	825.09	638.78	372.58	64.93	93.77
Th	0.02	0.01	0.02	0.27	0.16	0.18	0.06	0.04	0.08
Zr	0.05	0.13	/	14.24	1.43	0.41	0.76	0.13	0.09
Cr	1.28	0.31	1.24	1.16	1.51	1.73	1.61	1.12	0.45
Fe	75.12	97.17	71.04	520.96	283.9	217.17	239.71	117.99	102.47
Mo	0.41	0.56	1.11	2.29	2.92	2.86	6.16	6.14	3.29
Cu	0.06	0.07	0.2	0.93	0.47	0.37	0.83	0.31	0.04
La	0.09	0.06	0.05	1	0.52	0.58	0.27	0.57	0.74
Ce	0.14	0.19	0.16	1.61	1.13	1.15	0.52	1.42	1.88
Pr	0.04	0.03	0.03	0.23	0.09	0.18	0.02	0.13	0.2
Nd	0.13	0.1	0.09	0.49	0.33	0.56	0.21	0.55	0.56
Sm	—	—	0.03	0.2	0.06	0.15	0.12	0.23	0.08
Eu	—	0.01	0	0.03	0.01	0.01	0.01	0.02	0.01
Gd	—	0.02	0.03	0.24	0.12	0.02	—	0.03	0.15
Tb	0	—	—	0.04	0.02	0.01	0	0.02	0.01
Dy	0.01	0.01	0.02	0.17	0.13	0.09	0.04	0.03	0.07
Y	0.02	0.03	0.04	1.15	0.36	0.36	0.18	0.49	0.73
Ho	0.01	0	0	0.11	0.02	0.01	0.01	0.01	0.02
Er	0.01	0.01	0.01	0.1	0.03	0.02	0.02	0.04	0.04
Tm	—	0	—	0.05	0.01	0.01	—	0.01	—
Yb	—	—	—	0.22	0.06	0.03	0.05	0.04	0.05
Lu	—	—	0	0.01	0.01	0.01	0	0.01	0.01
$\Sigma REE+Y$	0.44	0.45	0.45	5.63	2.92	3.18	1.44	3.6	4.54
Nd_{SN}/Yb_{SN}	—	—	—	0.19	0.46	1.69	0.36	1.09	1
Ce/Ce^*	0.52	1.04	0.78	0.77	1.17	0.81	1.44	1.19	1.13
Eu/Eu^*	—	—	0.90	0.65	0.52	0.45	0.28	0.55	0.84
Mn/Sr	0.16	0.21	0.18	0.09	0.15	0.17	0.06	0.05	0.08

FIGURE 2
Geochemistry of specific components of microbialites and cathodoluminescence microphotos of Member IV of the Leikoupo Formation. **(A,D,G)** Laser ablation locations for specific components in Sample YaS-1, Ys-12, YaS-28, respectively; ① Microbial fabric, ② Transitional zone, ③ Fine spar fabric; **(B,E,H)** Shale-normalized REE+Y distribution patterns of specific components of Sample YaS-1, YS-12, YaS-28, respectively **(C,F,I)** Trace elements (Cr, Fe, Cu, Mo) of specific components in Sample YaS-1, YS-12, YaS-28, respectively.

transitional zone fabric, whereas the microbial and fine spar fabrics have similar Cr contents. In contrast to Cr, the transitional zone fabric has the highest Fe content, and the Fe concentration in the microbial fabric is slightly higher than that of the fine spar fabric. The highest Cu and Mo concentrations were found in the fine spar fabric, and the lowest values in the microbial fabric (Table 1; Figure 2C). In Sample YS-12 (stromatolite), the Cr concentrations increased from the microbial and transitional zone fabrics to the fine spar fabric, whereas the Fe and Cu concentrations decreased. The Mo concentration of the microbial fabric in Sample Ys-12 is lower than those of the transitional zone and fine spar fabrics (Table 1; Figure 2F). In Sample YaS-28 (grain dolostone), the Cr, Fe, and Cu concentrations decreased from the microbial and transitional zone fabrics to the fine spar fabric. The Mo concentrations of the microbial and transitional zone fabrics are similar, but higher than that of the fine spar fabric (Table 1; Figure 2I).
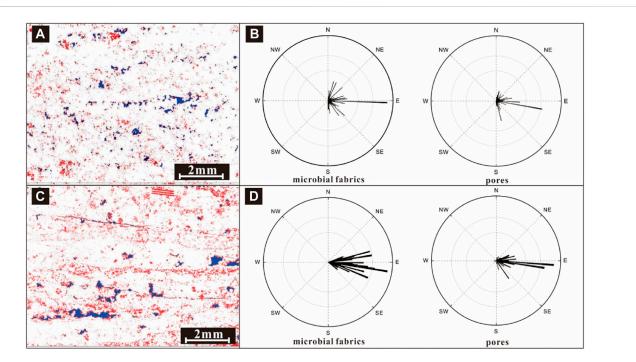
Rare earth element (REE) concentrations of the specific components in the microbialites were normalized to Post-Archean Australian Shale (PAAS; McLennan, 1989) and Ce anomalies were calculated as (Ce/Ce*) = 2 × Ce_{SN}/(La_{SN} + Pr_{SN}). In general, the microbialites in the Leikoupo Formation have low ΣREE+Y contents, which range from 0.439 to 5.629 ppm. Amongst the three analyzed samples, Sample YaS-1 has the lowest ΣREE+Y contents

(0.439–0.452 ppm). In Sample YaS-1, the microbial fabric has a negative Ce anomaly, whereas the transitional zone and fine spar fabrics have positive and slightly positive Ce anomalies, respectively. Sample YS-12 has the highest ΣREE+Y content. The microbial fabric is enriched in heavy REE (Nd_{SN}/Yb_{SN} = 0.18; Table 1) and has a negative Ce anomaly. The transitional zone fabric is also enriched in heavy REE (Nd_{SN}/Yb_{SN} = 0.46), but has a positive Ce anomaly. The fine spar fabric in Sample YS-12 exhibits depletion of heavy REE (Nd_{SN}/Yb_{SN} = 1.69) and a slightly positive Ce anomaly. In Sample YaS-28, the microbial fabric displays strong depletion in light REE (Nd_{SN}/Yb_{SN} < 1; Table 1), whereas the transitional zone and fine spar fabrics exhibit enrichment in heavy REE and positive Ce anomalies.

5 Discussion

5.1 Occurrence of pores and microbial fabrics

Quantitative statistical analysis of the two-dimensional spatial occurrence (size and orientation) of pores and microbial fabrics in the stromatolites and thrombolites was conducted on the 30 microbialite samples. In rose diagrams, it is clear that there is a good correlation between the orientations of pores and microbial

FIGURE 3
Quantitative statistics for occurrences (size and orientation) of pores and microbial fabrics in thrombolites and stromatolites showing close correlations between the pores and microbial fabrics. **(A,C)** Microphotos of thrombolite and stromatolite, respectively; the red area represents the microbial fabrics and the blue area represents the pores. **(B)** Rose diagram showing orientation and size of microbial fabrics and pores in thrombolites. **(D)** Rose diagram showing orientation and size of microbial fabrics and pores in stromatolites.

fabrics (Figure 3). In the thrombolites, pores are mainly located between the clots (Figure 3A), and the sizes and orientations of the clots coincide with those of the pores (Figure 3B). In the stromatolites, the pores are mainly developed between the laminations (Figure 3C), and the pores are arranged parallel to the laminations (Figure 3D). The excellent correlation between the pore orientations and microbial fabrics implies that the development of microbialite reservoir space might have been related to the microbial fabrics.

Previous studies have also shown that pores in microbialites are controlled by microbial fabrics (Rezende et al., 2013). The reservoir space in microbialites consists mainly of secondary dissolution pores, which are generated by the expanding dissolution of primary pores during later diagenesis, and the primary pores comprise mainly framework pores and micropores (Mancini et al., 2013). The formation of micropores in microbialites is related to organic matter mineralization (Pace et al., 2016). Chafetz (2013) studied micropores in travertine deposits and considered that micropores were formed *via* mineralization of organic matter. These micropores are expected to provide channels for meteoric fluids to dissolve carbonate minerals, and the pre-existing micropores can also grow during secondary dissolution processes (Zhao et al., 2014; Shen et al., 2015).

Quantitative measurement of the pore and microbial fabric areas in thin-section suggests there is no positive correlation between porosity and microbial fabric area (Table 2; Figure 4). Theoretically, when organic matter mineralization causes dissolution, the higher microbial fabric content will create more micropores and more intense secondary dissolution by later fluids. This might result in a positive correlation between porosity and the microbial fabric area. However, organic matter mineralization in

microbialtes could complicate this relationship because organic matter mineralization can result in either dissolution or cementation (Dupraz et al., 2009). When organic matter mineralization causes cementation, micropores will decrease and this will lead to a negative correlation between porosity and microbial fabric area. The lack of a correlation between porosity and microbial fabric area in this study might imply that the studied samples experienced different organic matter mineralization processes and amounts of secondary dissolution. Therefore, organic matter mineralization processes in microbialites are important in the development of microbialite reservoirs.
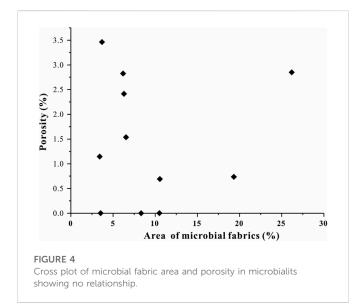
5.2 Organic matter mineralization in the microbialites

5.2.1 Evaluation of terrigenous contamination, secondary alteration, and dolomitization

Before using the LA–ICP–MS trace element data to investigate organic matter mineralization processes, potential contamination from terrigenous detrital material should be taken into account (Frimmel, 2009; Zhang et al., 2014). Marine sediments are complex mixtures of detrital and authigenic material (Goldberg, 1963), and each contributes trace elements to the total sediment inventory. The detrital fraction consists mainly of terrigenous material. The seawater-derived fraction accumulates as metal oxides, hydroxides, sulfides, and adsorbed phases (i.e., the hydrogenous fraction), and as $CaCO_3$. The composition of the detrital fraction reflects sediment provenance, whereas the composition of the seawater fraction reflects the depositional conditions and early diagenesis in the marine

TABLE 2 Area of microbial fabrics and pores in microbialites.

Samples	Lithology	Area of microbial fabrics (%)	Porosity (%)
YaS-1-01	thrombolite	10.6	0.7
YaS-1-04	thrombolite	3.7	3.5
YaS-2-02	thrombolite	3.4	1.1
YaS-13-05	thrombolite	6.5	1.5
YaS-20-01	thrombolite	10.5	0
YaS-34-02	thrombolite	3.5	0
YS-11-01	thrombolite	26.2	2.8
YS-13-01	thrombolite	19.3	0.7
YS-17-01	thrombolite	6.3	2.4
YS-12-02	stromatolite	8.3	0
YS-16-01	stromatolite	6.2	2.8

FIGURE 4
Cross plot of microbial fabric area and porosity in microbialits showing no relationship.
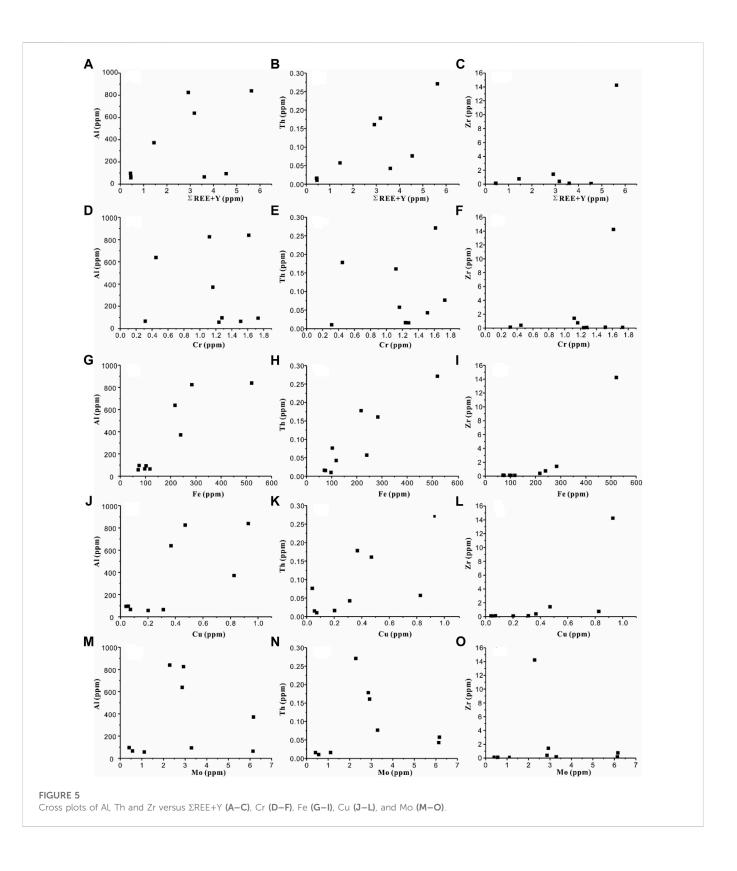
environment (Piper, 1994). Some high-field-strength elements, such as Al, Th, and Zr, can be used as useful tracers of the terrigenous detrital fraction (Goldstein and Jacobsen, 1988; Elderfield et al., 1990). A positive correlation is expected between ΣREE+Y, trace elements (Cr, Fe, Cu, and Mo), and Al, Th, and Zr concentrations, if there is contamination by terrigenous detrital material (Elderfield et al., 1990; Zhang et al., 2014). The studied samples have poor linear relationships between ΣREE+Y, trace elements (Cr, Fe, Cu, and Mo), and Al, Th, and Zr concentrations (Figure 5). In addition, the Al, Th, and Zr contents in the microbialites are mostly <839.5, <0.2, and <2 ppm, respectively (Table 1), indicating that the amount of terrigenous debris is <2%, according to their contents in the upper crust (Al, Th, and Zr concentrations of 80,312, 10.7, and 190 ppm, respectively; Taylor and McLennan, 1985). This suggests that the *in situ* geochemical data were not compromised by terrigenous detrital material.

Secondary alteration can also have a significant influence on trace elements. Studies of carbonate diagenesis in Phanerozoic rocks have generally observed elevated contents of Mn, Fe, and Zn, and

decreasing contents of Sr, Na, and Mg (Brand and Veizer, 1980). Because the partition coefficient for Sr between carbonate minerals and water $K_{mineral/water}$ is <1 and $K_{mineral/water}$ for Mn^{2+} is >1 (Banner, 1995), elevated Mn/Sr ratios suggest the influence of diagenetic overprinting (Popp et al., 1986; Fölling and Frimmel, 2002). The low Mn/Sr ratios of the present dataset (Mn/Sr < 0.3; Table 1) indicate there was little secondary alteration.

The analyzed microbial fabrics and cements are dolomitized. Microscopic observations show that these dolomites are micro-to finely crystalline, and have planar crystals (Figures 3, 6), indicating dolomitization at low temperatures during the early stages of diagenesis (Moore and Wade, 2013). This inference is confirmed by the high concentration of Na in all the analyzed samples (Table 1). Previous studies have proposed that the Na contents of dolomites in the early stages of diagenesis are higher than those in later stages (Brand and Veizer, 1980). The present data show that the Na concentrations of the microbial fabrics are significantly higher than modern seawater, ranging from 110 to 160 ppm (Veizer et al., 1999). However, the Na concentrations of the dolomite cements are similar to that of modern seawater. Furthermore, $\delta^{13}C$ and $\delta^{18}O$ values of micro- and finely crystalline dolomites of Member IV from the Leikoupo Formation in the studied area are 1‰–3‰ and −5‰–0‰, respectively (Lin, 2016; Jiang et al., 2018), which are consistent with those of global middle to upper Anisian (Middle Triassic) marine carbonates (−1.0‰ to −2.0‰ for $\delta^{13}C$ and −6.0‰ to −1.0‰ for $\delta^{18}O$) (Korte et al., 2005). Wang et al. (2018) showed that the early dolomite cement (Phase I) in Member IV of the Leikoupo Formation in the study area has a $\delta^{13}C$ value of 1.29‰ and $\delta^{18}O$ value of −5.11‰, which are within the ranges of contemporaneous-penecontemporaneous marine carbonates. Therefore, the analyzed micro- and finely crystalline dolomites and dolomitic cements are inferred to have been dolomitized by seawater at low temperatures. In addition, cathodoluminescence (CL) imaging showed that the micro- and finely crystalline dolomites and cements are not luminescent (Figure 2). This is consistent with the high Fe and low Mn contents of the samples (Table 1).
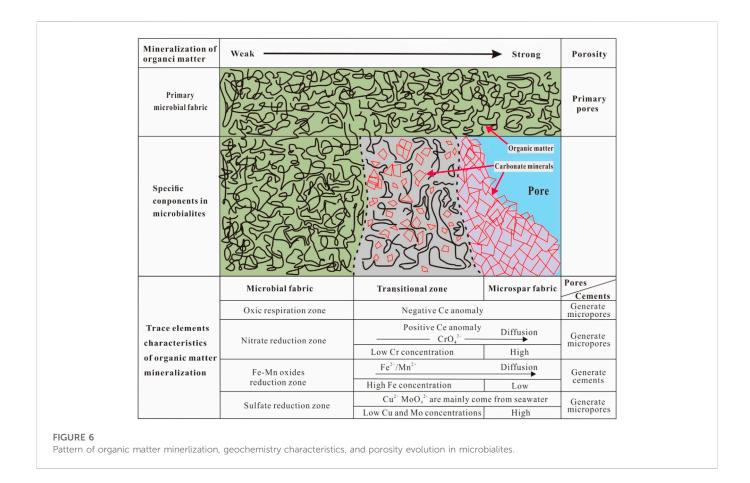
In summary, the analyzed micro- and finely crystalline dolomites and cements were mainly dolomitized by seawater at low temperatures and in early diagenetic stage, and were not subjected to later secondary

FIGURE 5
Cross plots of Al, Th and Zr versus ΣREE+Y **(A–C)**, Cr **(D–F)**, Fe **(G–I)**, Cu **(J–L)**, and Mo **(M–O)**.

alteration. The trace element data were also not affected by terrigenous detrital material and, therefore, are suitable for the study of early diagenesis in a marine environment (Nothdurft et al., 2004).

5.2.2 Organic matter mineralization processes

In order to decipher the organic matter mineralization processes in microbialites with different porosities (YaS-1, YS-12, and YaS-28),

LA–ICP–MS was used to analyze the trace elements of specific components in the microbialites (i.e., microbial, transitional zone, and fine spar fabrics). The trace element contents of cement and remnant dissolution components during organic matter mineralization are proxies for this process (Lovley, 1991; Piper, 1994; Madigan et al., 1997; Algeo and Maynard, 2004; Audry et al., 2011).

FIGURE 6
Pattern of organic matter minerlization, geochemistry characteristics, and porosity evolution in microbialites.

The Ce anomaly is an important proxy for determining redox conditions during deposition and organic matter mineralization. Ce^{3+} can be oxidized to Ce^{4+} in the modern ocean (Alibo and Nozaki, 1999) and absorbed onto the surface of Fe–Mn oxides in the form of $Ce(OH)_4$ or CeO_2. Therefore, Ce is sequestered from seawater, which results in negative Ce anomalies in seawater and microbial carbonates (Alibo and Nozaki 1999; Guo et al., 2007; Tostevin et al., 2016). The aerobic degradation of organic matter in microbialites typically occurs after deposition and above the oxidation–reduction interface (Oschmann, 2000; Dupraz and Visscher, 2005). The pore water actively exchanges with seawater and is still in an oxic state and, therefore, carbonate minerals precipitated from pore waters generally have a negative Ce anomaly similar to seawater (Figure 6). When the microbialites are beneath the oxidation–reduction interface, the pore water is in a weakly reduced to reduced state, where organic matter will undergo anaerobic degradation. In this case, Ce in the pore water is reduced to Ce^{3+} and can substitute for cations (e.g., Ca^{2+} and Mg^{2+}) in carbonate minerals (Tostevin et al., 2016), which results in the positive Ce anomalies of the transitional zone and fine spar fabrics in the microbialites (Figure 6).

The microbial fabrics of Samples YaS-1 (thrombolite) and YS-12 (stromatolite) have negative Ce anomalies (Table 1; Figure 2), indicating these microbialites formed in oxic seawater. However, the transitional zone and fine spar fabrics in all three samples have positive Ce anomalies, implying that the organic matter in all three samples had undergone aerobic respiration and begun anaerobic degradation.

If organic matter is not entirely consumed during aerobic respiration, it will be oxidized further by NO_3^- and CrO_4^{2-} in the nitrate reduction zone (Richard and Bourg, 1991; Oschmann, 2000; Widdicombe et al., 2011). During this process, CrO_4^{2-} can be reduced to Cr^{3+}, and Cr^{3+} combines with OH^- to precipitate $Cr(OH)_3$ (Algeo and Maynard, 2004), and result in Cr concentrations of the fine spar fabrics will be higher than those of transitional zone fabrics (Figs 9 and Figs 11). Therefore, the concentration of Cr in fine spar and transitional zone fabrics can trace the procession of organic matter oxidization by NO_3^-.

The Cr concentrations of the fine spar fabrics in Samples Yas-1 and YS-12 (1.24–1.73 ppm, respectively) are significantly higher than those of the transitional zone fabrics (0.31–1.51 ppm, respectively; Table 1; Figure 2), indicating that organic matter in these two samples was mineralized by NO_3^- and CrO_4^{2-}. However, the Cr concentration of the fine spar fabric in Sample YaS-28 is lower than that of the transitional zone (Table 1; Figure 2), demonstrating that organic matter in Sample YaS-28 was not mineralized by CrO_4^{2-}, and that organic matter mineralization probably ceased in the nitrate reduction zone.

Organic matter will be oxidized by Fe^{3+} and Mn^{4+} oxides when they are buried deeply. Fe^{3+} and Mn^{4+} oxides can be reduced to Fe^{2+} and Mn^{2+} and migrate from sediments to pore water during organic matter mineralization in the Fe–Mn oxide reduction zone (Lovley, 1991; Canfield et al., 1993). Organic matter mineralization will results in the lower Fe concentration in the fine spar fabric compared with the transitional zone fabric (Figures 2 and 6). Iron concentrations of the transitional zone fabrics in Samples YS-12 and YaS-1 (284 and 97.2 ppm, respectively) are higher than those of the fine spar fabrics (217 and 71.0 ppm, respectively), indicating that organic

TABLE 3 Reactions of organic matter mineralization and pore development.

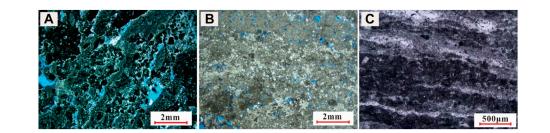| Reactions of organic matter mineraliation	Ratio of OM to pore in each reaction	Cumulative ratio of OM to pore
Aerobic respiration: $CH_2O + O_2 + CaCO_3 \rightarrow 2HCO_3^- + Ca^{2+}$	1:2	1:2
Nitrate reduction: $5CH_2O + 4NO_3^- + CaCO_3 \rightarrow 6HCO_3^- + 2N_2 + 2H_2O + Ca^{2+}$	5:6	1:1.6
Fe-Mn oxides reduction: $CH_2O + 4FeOOH + 6HCO_3^- + 7Ca^{2+} \rightarrow 7CaCO_3 + 4Fe^{2+} + 6H_2O$	1:−6	1:−0.93
Sulfate reduction: $2CH_2O + SO_4^{2-} + OH^- + Ca^{2+} \rightarrow CaCO_3 + CO_2 + 2H_2O + HS^-$	2:1	1:−0.57

FIGURE 7
Microphotos showing three microbialites with different porosity. The blue area represents pores. **(A)** Sample YaS-28 has the highest porosity value of 9.11%; **(B)** Sample YaS-1 has moderate porosity value of 4.91%; **(C)** Sample YS-12 has lowest porosity value of 0.12%.

matter in these samples was mineralized by Fe–Mn oxides. However, Fe concentrations of the transitional zone and fine spar fabrics are broadly similar to those of the microbial fabric in Sample YaS-1 (Table 1; Figure 2), suggesting that organic matter in this sample was not extensively mineralized by Fe–Mn oxides. In Sample YaS-28, the transitional zone and fine spar fabrics have approximately the same Fe contents (Table 1; Figure 2), indicating that organic matter in Sample YaS-28 was not mineralized by Fe–Mn oxides. This is consistent with the conclusion that organic matter mineralization in Sample YaS-28 ceased in the nitrate reduction zone.

After degradation in the Fe–Mn oxide reduction zone, the remnant organic matter may be further mineralized in the sulfate reduction zone (Froelich et al., 1979; Canfield and Thamdrup, 2009). In the sulfate reduction zone, sulfate can be reduced to bivalent sulfur in the pore water, which reacts with Cu^{2+} and MoO_4^{2-} to form insoluble CuS and MoS_2 (Fig. 9; Piper, 1994; Scott et al., 2008). The concentrations of Mo and Cu in the fine spar fabric will be indeed higher than those in the transitional zone fabric (Figure 6). In Sample YaS-1, the Cu and Mo concentrations of the fine spar fabric are higher than those of the transitional zone fabric (Table 1; Figure 2), suggesting that organic matter mineralization in this sample involved sulfate reduction. In Sample YS-12, the Cu and Mo concentrations of the fine spar fabric are lower than those of the transitional zone fabric (Table 1; Figure 2), which may be related to the absence of free H_2S in the pore water.

In summary, there are subtle differences in the processes of organic matter mineralization in microbialites with different porosities in Member IV of the Leikoupo Formation. The organic matter in Sample YaS-28 (grain dolostone) was mineralized by oxidation and nitrate reduction. The organic matter in Sample YS-12 (stromatolite) was mineralized by oxidation, and nitrate and Fe–Mn oxide reduction. The organic matter in Sample YaS-1 (thrombolite) was mineralized by

oxidation, and nitrate, Fe–Mn oxide, and sulfate reduction, but only to a limited extent in the Fe–Mn oxide reduction zone.

5.3 Implications of organic matter mineralization for reservoir development

Organic matter mineralization by aerobic respiration and nitrate reduction will result in the dissolution of carbonate minerals and create micropores, whereas mineralization by Fe–Mn oxides and sulfates will precipitate carbonate minerals and block pores (Froelich et al., 1979; Visscher and Stolz, 2005). To simply and qualitatively evaluate the impact of organic matter mineralization on the development of a microbialite reservoir, it was assumed that 1 mol of organic matter (CH_2O; expressed here in its simplest form) is equivalent to 1 mol of $CaCO_3$ in volume. Volume ratios of organic matter to pores of each mineralization reaction and cumulative ratios of organic matter to pores for the total mineralization process are summarized in Table 3. For example, mineralization by aerobic respiration leads to one unit of $CaCO_3$ being dissolved for every unit of organic matter consumed. Thus, two units of pores are created by this mineralization, and the volume ratio of organic matter to pores during mineralization by aerobic respiration is 1:2 (Table 3).

The highest volume ratio of pores to organic matter is reached when the organic matter is mineralized in the nitrate reduction zone (excluding aerobic respiration) (Table 3). This means that microbialites in which organic matter has been mineralized by oxidation and nitrate reduction are likely to contain the largest volume of micropores, which act as fluid channels for later fluid dissolution, and likely become the best reservoirs. Sample YaS-28

experienced organic matter mineralization by oxidation and nitrate reduction and has the greatest pore development (porosity = 9.11%) amongst the three analyzed samples (Figure 7A). The porosity development in Sample YaS-28 might be due to a large number of pre-existing micropores, which were created by organic matter mineralization in the aerobic respiration and nitrate reduction zones. At the end of the Ladinian stage, Indosinian tectonism resulted in Member IV of the Leikoupo Formation being exposed at the surface (Zhong et al., 2011; Tang, 2013; Tan et al., 2014), and meteoric water dissolved the rock along pre-existing micropores, generating a large number of dissolution pores in the grain dolostones.

As the organic matter mineralization proceeded further and into the Fe–Mn oxide reduction zone, $CaCO_3$ cementation occurred (Zeng and Tice, 2014). The micropores created by the process of aerobic respiration and nitrate reduction would have become filled, and the cumulative ratio of organic matter to pores reached its lowest value of 1:−0.93 (Table 3). Cement produced in this process might hinder later dissolution. If there was remnant organic matter after mineralization in the Fe–Mn oxide reduction zone, then the organic matter will be further mineralized in the sulfate reduction zone when the microbialites are deeply buried (Canfield and Thamdrup, 2009; Schunck et al., 2013; Li et al., 2015). In the sulfate reduction zone, organic matter mineralization will elevate the cumulative ratio of organic matter to pores from 1:−0.93 to 1:−0.57, even though the sulfate reduction process will cause carbonate mineral precipitation (Table 3).

The *in situ* geochemical data suggest that the organic matter in Sample YS-12 (stromatolite) underwent extensive mineralization by Fe–Mn oxides but not by sulfate. Considering the cumulative ratio of organic matter to pores is 1:−0.93 in the Fe–Mn oxide reduction zone (Table 3), organic matter mineralization in Sample YS-12 would have produced cement, thereby hindering subsequent dissolution and pore expansion. As such, the lowest porosity of Sample YS-12 (0.12%) may be related to its organic matter mineralization (Figure 7C). In contrast, the organic matter in Sample YaS-1 (thrombolite) was mineralized by aerobic respiration, nitrate reduction, limited Fe–Mn oxide reduction, and sulfate reduction. The final cumulative ratio of organic matter to pores in Sample YaS-1 should be between 0 and 1:1.6 (Table 3). Thus, organic matter mineralization in Sample YaS-1 did create micropores, and these micropores acted as channels for meteoric water for dissolution during subsequent karstification. Consequently, Sample YaS-1 has a porosity of 4.91% (Figure 7B).

It is clear that organic matter mineralization processes have a significant impact on the development of microbialite reservoirs. Micropores created by mineralization of organic matter in microbialites can provide channels for fluids and are also favorable sites for later dissolution. However, if organic matter mineralization produces cement, these cements may prevent the development of a microbialite reservoir. It should be noted that the micropores created by organic matter mineralization are almost always micron-sized (Chafetz, 2013) and make a limited contribution to reservoir space, but they can act as channels for fluid dissolution and accelerate karstification.

6 Conclusion

Organic matter in microbialites can be oxidised by oxygen, NO3−, CrO42−, Fe–Mn oxide and by sulfates. Preliminary *in situ* geochemical analyses can trace these organic matter mineralization processes by Ce anomalies and Cr, Cu and Mo concentrations in different microbial components and fabrics. It is proposed that organic matter mineralization creates micropores that may have acted as fluid channels for later dissolution that developed good reservoirs. However, these micropores contribute limited space to the microbialite reservoir. In contrast, organic matter mineralization associated with cementation will hinder the development of a microbialite reservoir.

Data availability statement

The original contributions presented in the study are included in the article/Supplementary Material, further inquiries can be directed to the corresponding author.

Author contributions

YZ finished the manuscript; KL, ZZ, YQ, GS, LZ, and BZ took part in discussion in the manuscript; YW, SD, WY, and JY collected the samples and finished the graphs; JY finished the manuscript and gave the final conclusion.

Conflict of interest

Authors YZ, KL, ZZ, YQ, GS, LZ, BZ, YW, SD, and WY were employed by PetroChina Southwest Oil and Gasfield Company.

The remaining author declares that the research was conducted in the absence of any commercial or financial relationships that could be construed as a potential conflict of interest.

Publisher's note

All claims expressed in this article are solely those of the authors and do not necessarily represent those of their affiliated organizations, or those of the publisher, the editors and the reviewers. Any product that may be evaluated in this article, or claim that may be made by its manufacturer, is not guaranteed or endorsed by the publisher.

References

Algeo, T. J., and Maynard, J. B. (2004). Trace-element behavior and redox facies in core shales of Upper Pennsylvanian Kansas-type cyclothems. *Chem. Geol.* 206, 289–318. doi:10.1016/j.chemgeo.2003.12.009

Alibo, D. S., and Nozaki, Y. (1999). Rare Earth elements in seawater: Particle association, shale-normalization, and Ce oxidation. *Geochimica Cosmochimica Acta* 63, 363–372. doi:10.1016/s0016-7037(98)00279-8

Audry, S., Pokrovsky, O. S., Shirokova, L. S., Kirpotin, S. N., and Dupré, B. (2011). Organic matter mineralization and trace element post-depositional redistribution in Western Siberia thermokarst lake sediments. *Biogeosciences* 8, 3341–3358. doi:10.5194/bg-8-3341-2011

Banner, J. L. (1995). Application of the trace element and isotope geochemistry of strontium to studies of carbonate diagenesis. *Sedimentology* 42, 805–824. doi:10.1111/j.1365-3091.1995.tb00410.x

Brand, U., and Veizer, J. (1980). Chemical diagenesis of a multicomponent carbonate system; 1, Trace elements. *J. Sediment. Res.* 50, 1219–1236.

Canfield, D. E. (1991). Sulfate reduction in deep-sea sediments. *Am. J. Sci.* 291, 177–188. doi:10.2475/ajs.291.2.177

Canfield, D. E., Thamdrup, B., and Hansen, J. W. (1993). The anaerobic degradation of organic matter in Danish coastal sediments: Iron reduction, manganese reduction, and sulfate reduction. *Geochimica Cosmochimica Acta* 57, 3867–3883. doi:10.1016/0016-7037(93)90340-3

Canfield, D. E., and Thamdrup, B. (2009). Towards a consistent classification scheme for geochemical environments, or, why we wish the term 'suboxic' would go away. *Geobiology* 7, 385–392. doi:10.1111/j.1472-4669.2009.00214.x

Chafetz, H. S. (2013). Porosity in bacterially induced carbonates: Focus on micropores. *AAPG Bull.* 97, 2103–2111. doi:10.1306/04231312173

Chen, Y. N., Shen, A. J., Pan, L. Y., Zhang, J., and Wang, X. F. (2017). Features, origin and distribution of microbial dolomite reservoirs: A case study of 4th member of sinian Dengying Formation in Sichuan Basin, SW China. *Petroleum Explor. Dev.* 44, 745–757. doi:10.1016/s1876-3804(17)30085-x

Decho, A. W., Visscher, P. T., and Reid, R. P. (2015). Production and cycling of natural microbial exopolymers (EPS) within a marine stromatolite. *Palaeogeogr. Palaeoclimatol. Palaeoecol.* 219, 71–86. doi:10.1016/j.palaeo.2004.10.015

Ding, X., Tan, X. C., Li, L., Luo, B., Tang, Q. S., and Ma, H. L. (2013). Characteristics and genetic analysis of grain shoal reservoirs in member III of middle triassic Leikoupo Formation, Sichuan Basin. *J. China Univ. Petroleum Ed. Nat. Sci.* 37, 30–37. doi:10.3969/j.issn.1673-5005.2013.04.005

Dupraz, C., Reid, R. P., Braissant, O., Decho, A. W., Norman, R. S., and Visscher, P. T. (2009). Processes of carbonate precipitation in modern microbial mats. *Earth-Science Rev.* 96, 141–162. doi:10.1016/j.earscirev.2008.10.005

Dupraz, C., and Visscher, P. T. (2005). Microbial lithification in marine stromatolites and hypersaline mats. *Trends Microbiol.* 13, 429–438. doi:10.1016/j.tim.2005.07.008

Elderfield, H., Upstill-Goddard, R., and Sholkovitz, E. R. (1990). The rare Earth elements in rivers, estuaries, and coastal seas and their significance to the composition of ocean waters. *Geochimica Cosmochimica Acta* 54, 971–991. doi:10.1016/0016-7037(90)90432-k

Fölling, P. G., and Frimmel, H. E. (2002). Chemostratigraphic correlation of carbonate successions in the gariep and saldania belts, Namibia and south Africa. *Basin Res.* 14, 69–88. doi:10.1046/j.1365-2117.2002.00167.x

Frimmel, H. E. (2009). Trace element distribution in Neoproterozoic carbonates as palaeoenvironmental indicator. *Chem. Geol.* 258 (3-4), 338–353. doi:10.1016/j.chemgeo.2008.10.033

Froelich, P., Klinkhammer, G. P., Bender, M. L., Luedtke, N. A., Heath, G. R., Cullen, D., et al. (1979). Early oxidation of organic matter in pelagic sediments of the eastern equatorial atlantic: Suboxic diagenesis. *Geochimica Cosmochimica Acta* 43, 1075–1090. doi:10.1016/0016-7037(79)90095-4

Glunk, C., Dupraz, C., Braissant, O., Gallagher, K. L., Verrecchia, E. P., and Visscher, P. T. (2011). Microbially mediated carbonate precipitation in a hypersaline lake, Big Pond (Eleuthera, Bahamas). *Sedimentology* 58, 720–736. doi:10.1111/j.1365-3091.2010.01180.x

Goldberg, E. D. (1963). Mineralogy and chemistry of marine sedimentation. *Submar. Geol.* 1963, 436–466.

Goldstein, S. J., and Jacobsen, S. B. (1988). Rare Earth elements in river waters. *Earth Planet. Sci. Lett.* 89, 35–47. doi:10.1016/0012-821x(88)90031-3

Guo, Q., Shields, G. A., Liu, C., Strauss, H., Zhu, M., Pi, D., et al. (2007). Trace element chemostratigraphy of two ediacaran–cambrian successions in south China: Implications for organosedimentary metal enrichment and silicification in the early cambrian. *Palaeogeogr. Palaeoclimatol. Palaeoecol.* 254, 194–216. doi:10.1016/j.palaeo.2007.03.016

Guo, Z. W., Deng, K. L., Han, Y. H., Liu, Y. K., Yin, J. T., Wang, Q. G., et al. (2004). Rare Earth elements in pore waters of marine sediments. *Geochimica Cosmochimica Acta* 68, 1265–1279. doi:10.1016/j.gca.2003.09.012

Harwood, C. L., and Sumner, D. Y. (2011). Microbialites of the neoproterozoic beck spring dolomite, southern California. *Sedimentology* 58, 1648–1673. doi:10.1111/j.1365-3091.2011.01228.x

Huang, D., Zhang, J., Yang, G., Shi, X. W., and Wang, H. (2011). The discussion of stratum division and stratum for the Leikoupo Formation of middle triassic in Sichuan Basin. *J. Southwest Petroleum Univ. Sci. Technol. Ed.* 33, 89–95. doi:10.3863/j.issn.1674-5086.2011.03014

Ingalls, A. E., Aller, R. C., Lee, C., and Wakeham, S. G. (2004). Organic matter diagenesis in shallow water carbonate sediments. *Geochimica Cosmochimica Acta* 68, 4363–4379. doi:10.1016/j.gca.2004.01.002

Jiang, L., Hu, S., Zhao, W., Xu, Z., Shi, S., Fu, Q., et al. (2018). Diagenesis and its impact on a microbially derived carbonate reservoir from the middle triassic Leikoupo Formation, Sichuan Basin, China. *AAPG Bull.* 102, 2599–2628. doi:10.1306/05111817021

Korte, C., Kozur, H. W., and Veizer, J. (2005). $\delta^{13}C$ and $\delta^{18}O$ values of Triassic brachiopods and carbonate rocks as proxies for coeval seawater and palaeotemperature. *Palaeogeogr. Palaeoclimatol. Palaeoecol.* 226, 287–306. doi:10.1016/j.palaeo.2005.05.018

Li, C., Cheng, M., Algeo, T. J., and Xie, S. (2015a). A theoretical prediction of chemical zonation in early oceans (>520 Ma). *Sci. China Earth Sci.* 58, 1901–1909. doi:10.1007/s11430-015-5190-7

Li, L., Tan, X. C., Cao, J., Zou, C., Ding, X., Yang, G., et al. (2014). Origins of evaporites in the middle triassic Leikoupo Formation of the Sichuan Basin, southwest China and their geological implications. *Carbonates Evaporites* 29, 55–63. doi:10.1007/s13146-013-0169-y

Li, P. W., Luo, P., Chen, M., Song, J. M., Jin, T. F., and Wang, G. Q. (2015b). Characteristics and main controlling factors of microbial carbonate reservoirs: A case study of upper sinian-lower cambrian in the northwestern margin of tarim basin. *Acta Pet. Sin.* 36, 1074–1108. doi:10.7623/syxb201509005

Li, S., Xu, G., and Song, X. (2016). Forming conditions of Pengzhou large gas field of Leikoupo Formation in Longmenshan piedmont tectonic belt, Western Sichuan Basin. *China Pet. Explor.* 21, 74–82. doi:10.3969/j.issn.1672-7703.2016.03.007

Lin, T. (2016). *Reservoir characteristics of middle triassic member IV of Leikoupo Formation in the central part of western Sichuan Basin* (Chendu: Chengdu Univerisity of Technology), 1–97. doi:10.3969/j.issn.1671-9727.2016.02.01

Liu, S. G., Song, J. M., Luo, P., Hairuo, Q., Lin, T., Sun, W., et al. (2016). Characteristics of microbial carbonate reservoir and its hydrocarbon exploring outlook in the Sichuan Basin, China. *J. Chengdu Univ. Technol. Sci. Technol. Ed.* 43, 129–152.

Liu, X. Z. (1983). Characteristics and environmental significance of Middle Triassic Cryptoalgal carbonates in the northwestern part of Sichuan. *Acta Sedimentol. Sin.* 1, 79–87.

Liu, Y., Hu, Z., Gao, S., Günther, D., Xu, J., Gao, C., et al. (2008). *In situ* analysis of major and trace elements of anhydrous minerals by LA-ICP-MS without applying an internal standard. *Chem. Geol.* 257, 34–43. doi:10.1016/j.chemgeo.2008.08.004

Lovley, D. R. (1991). Dissimilatory Fe (III) and Mn (IV) reduction. *Microbiol. Rev.* 55, 259–287. doi:10.1128/mr.55.2.259-287.1991

Madigan, M. T., Martinko, J. M., and Parker, J. (1997). *Brock biology of microorganisms*. 8th ed. NJUpper Saddle River: Prentice-Hall.

Mancini, E. A., Morgan, W. A., Harris, P. M., and Parcell, W. C. (2013). Introduction: AAPG hedberg research conference on microbial carbonate reservoir characterization-conference summary and selected papers. *AAPG Bull.* 97, 1835–1847. doi:10.1306/intro070913

McLennan, S. M. (1989). Rare Earth elements in sedimentary rocks: Influence of provenance and sedimentary processes. *Geochem. Mineralogy Rare Earth Elem. Rev. Mineralogy* 21, 169–200.

Moore, C. H., and Wade, W. J. (2013). *Carbonate reservoirs: Porosity and diagenesis in a sequence stratigraphic framework* (Amsterdam: Elsevier), 1–160.

Nothdurft, L. D., Webb, G. E., and Kamber, B. S. (2004). Rare Earth element geochemistry of late devonian reefal carbonates, canning basin, western Australia: Confirmation of a seawater REE proxy in ancient limestones. *Geochimica Cosmochimica Acta* 68, 263–283. doi:10.1016/s0016-7037(03)00422-8

Oschmann, W. (2000). "Microbes and black shales," in *Microbial sediments*. Editors R. Riding and S. Awramik (Berlin: Springer), 137–148.

Pace, A., Bourillot, R., Bouton, A., Vennin, E., Galaup, S., Bundeleva, I., et al. (2016). Microbial and diagenetic steps leading to the mineralisation of Great Salt Lake microbialites. *Sci. Rep.* 6, 31495. doi:10.1038/srep31495

Peng, J. S., Liu, S. G., Zhang, C. J., Zhang, C. R., and Zhang, J. T. (2014). Study on diagenetic heterogeneity of the middle triassic Leikoupo Formation in front area of longmenshan mountains. *J. Palaeogeogr.* 16, 790–801. doi:10.7605/gdlxb2014.06.063

Piper, D. Z. (1994). Seawater as the source of minor elements in black shales, phosphorites and other sedimentary rocks. *Chem. Geol.* 114, 95–114. doi:10.1016/0009-2541(94)90044-2

Popp, B. N., Anderson, T. F., and Sandberg, P. A. (1986). Textural, elemental, and isotopic variations among constituents in Middle Devonian limestones, North America. *J. Sediment. Res.* 56, 715–727.

Raiswell, R., and Fisher, Q. J. (2004). Rates of carbonate cementation associated with sulphate reduction in DSDP/ODP sediments: Implications for the formation of concretions. *Chem. Geol.* 211, 71–85. doi:10.1016/j.chemgeo.2004.06.020

Rezende, M. F., and Pope, M. C. (2015). Importance of depositional texture in pore characterization of subsalt microbialite carbonates, offshore Brazil. *Geol. Soc. Lond. Spec. Publ.* 418, 193–207. doi:10.1144/sp418.2

Rezende, M. F., Tonietto, S. N., and Pope, M. C. (2013). Three-dimensional pore connectivity evaluation in a Holocene and Jurassic microbialite buildup. *AAPG Bull.* 97, 2085–2101. doi:10.1306/05141312171

Richard, F. C., and Bourg, A. C. (1991). Aqueous geochemistry of chromium: A review. *Water Res.* 25, 807–816. doi:10.1016/0043-1354(91)90160-r

Riding, R. (2000). Microbial carbonates: The geological record of calcified bacterial-algal mats and biofilms. *Sedimentology* 47, 179–214. doi:10.1046/j.1365-3091.2000.00003.x

Schunck, H., Lavik, G., Desai, D. K., Großkopf, T., Kalvelage, T., Löscher, C. R., et al. (2013). Giant hydrogen sulfide plume in the oxygen minimum zone off Peru supports chemolithoautotrophy. *PLoS One* 8 (8), e68661. doi:10.1371/journal.pone.0068661

Scott, C., Lyons, T. W., Bekker, A., Shen, Y. A., Poulton, S. W., Chu, X. L., et al. (2008). Tracing the stepwise oxygenation of the Proterozoic ocean. *Nature* 452 (7186), 456–459. doi:10.1038/nature06811

Shaw, T. J., Gieskes, J. M., and Jahnke, R. A. (1990). Early diagenesis in differing depositional environments: The response of transition metals in pore water. *Geochimica Cosmochimica Acta* 54, 1233–1246. doi:10.1016/0016-7037(90)90149-f

Shen, A. J., Zhao, W. Z., Hu, A. P., She, M., Chen, Y. N., and Wang, X. F. (2015). Major factors controlling the development of marine carbonate reservoirs. *Petroleum Explor. Dev.* 42, 597–608. doi:10.1016/s1876-3804(15)30055-0

Song, J. M., Liu, S. G., Li, Z. W., Luo, P., Yang, D., Sun, W., et al. (2017). Characteristics and controlling factors of microbial carbonate reservoirs in the upper sinian Dengying Formation in the Sichuan Basin, China. *Oil Gas Geol.* 38, 741–752. doi:10.11743/ogg20170411

Song, J. M., Luo, P., Yang, S. S., Yang, D., Zhou, C. M., Li, P. W., et al. (2014). Reservoirs of lower cambrian microbial carbonates, tarim basin, NW China. *Petroleum Explor. Dev.* 41, 449–459. doi:10.1016/s1876-3804(14)60051-3

Song, X., Wang, Q., Long, K., Xu, G., Shi, G., XiaFeng, X., et al. (2013). Characteristics and main controlling factors of middle triassic Leikoupo paleokarst reservoirs in western Sichuan Basin. *Mar. Orig. Pet. Geol.* 18, 8–14. doi:10.3969/j.issn.1672-9854.2013.02.002

Tan, X. C., Li, L., Liu, H., Cao, J., Wu, X. Q., Zhou, S. Y., et al. (2014). Mega-shoaling in carbonate platform of the middle Triassic Leikoupo formation, Sichuan Basin, southwest China. *Sci. China Earth Sci.* 57, 465–479. doi:10.1007/s11430-013-4667-5

Tang, Y. (2013). Characterization of the sedimentation of the Leikoupo Formation and the weathering crust reservoirs at the top of the formation in the Western Sichuan Basin. *Oil Gas Geol.* 34, 42–47.

Taylor, S. R., and Mclennan, S. M. (1985). The continental crust: Its composition and evolution. *J. Geol.* 94, 57–72.

Tostevin, R., Shields, G. A., Tarbuck, G. M., He, T., Clarkson, M. O., and Wood, R. A. (2016). Effective use of cerium anomalies as a redox proxy in carbonate-dominated marine settings. *Chem. Geol.* 438, 146–162. doi:10.1016/j.chemgeo.2016.06.027

Veizer, J., Ala, D., Azmy, K., Bruckschen, P., Buhl, D., Bruhn, F., et al. (1999). $^{87}Sr/^{86}Sr$, $\delta^{13}C$ and $\delta^{18}O$ evolution of Phanerozoic seawater. *Chem. Geol.* 161, 59–88. doi:10.1016/s0009-2541(99)00081-9

Visscher, P. T., and Stolz, J. F. (2005). Microbial mats as bioreactors: Populations, processes, and products. *Palaeogeogr. Palaeoclimatol. Palaeoecol.* 219, 87–100. doi:10.1016/j.palaeo.2004.10.016

Wang, H. (2018). The characteristics and main controlling factors of the fourth member of Middle Triassic Leikoupo Formation microbialite reservoir in the Western Sichuan Basin (Chendu: Chengdu University of Technology), 1–120.

Wang, Q., Song, X., Chen, H., and Liu, H. (2018). Cement characteristics and effects on dolomite reservoir pores in the fourth member of Leikoupo Formation, Longmen Mountain front, Western Sichuan Basin. *Petroleum Geol. Exp.* 40, 757–763. doi:10.11781/sysydz201806757

Wang, Q. X., Song, X. B., Wang, D., and Long, K. (2017). Reservoir characteristics and formation mechanism of the member IV of the Leikoupo Formation in longmen mountain front. *Petroleum Geol. Exp.* 39, 491–497.

Webb, E. G., and Kamber, B. S. (2004). Biogenicity inferred from microbialite geochemistry. *Microbiol. Aust.* 25, 34–35. doi:10.1071/ma04134

Webb, E. G., and Kamber, B. S. (2011). "Trace element Geochemistry as a tool for interpreting microbialites," in *Earliest life on earth: Habitats, environments and methods of detection*. Editors S. D. Golding and M. Glikson (Dordrecht: Springer), 127–170.

Widdicombe, S., Spicer, J. I., and Kitidis, V. (2011). "Effects of ocean acidification on sediment fauna," in *Ocean acidification* (Oxford: Oxford University Press), 176–191.

Wu, S. X., Li, H. T., Long, S. X., Li, Z. L., Wang, C. L., and Zhang, J. T. (2011). A study on characteristics and diagenesis of carbonate reservoirs in the middle triassic Leikoupo Formation in Western sichuan depression. *Oil Gas Geol.* 32, 542–550.

Zeng, Z., and Tice, M. M. (2014). Promotion and nucleation of carbonate precipitation during microbial iron reduction. *Geobiology* 12, 362–371. doi:10.1111/gbi.12090

Zhang, P., Hua, H., and Liu, W. (2014a). Isotopic and REE evidence for the paleoenvironmental evolution of the late ediacaran dengying section, ningqiang of shaanxi Province, China. *Precambrian Res.* 242, 96–111. doi:10.1016/j.precamres.2013.12.011

Zhang, W., Guan, P., Jian, X., Feng, F., and Zou, C. (2014b). *In situ* geochemistry of Lower Paleozoic dolomites in the northwestern Tarim basin: Implications for the nature, origin, and evolution of diagenetic fluids. *Geochem. Geophys. Geosystems* 15, 2744–2764. doi:10.1002/2013gc005194

Zhao, C. (2020). Characteristics of microbialites reservoir of Leikoupo Formation in the Western Sichuan Basin (Chendu: Chengdu University of Technology), 1–56.

Zhao, W. Z., Shen, A. J., Zhou, J. G., Wang, X. F., and Lu, J. M. (2014). Types, characteristics, origin and exploration significance of reef-shoal reservoirs: A case study of tarim basin, NW China and Sichuan Basin, SW China. *Petroleum Explor. Dev.* 41, 283–293. doi:10.1016/s1876-3804(14)60034-3

Zheng, Y., Anderson, R. F., Van Geen, A., and Kuwabara, J. (2000). Authigenic molybdenum Formation in marine sediments: A link to pore water sulfide in the santa barbara basin. *Geochimica Cosmochimica Acta* 64, 4165–4178. doi:10.1016/s0016-7037(00)00495-6

Zhong, Y. J., Chen, H. D., Lin, L. B., Hou, M. C., Li, X. H., Xu, S. L., et al. (2011). Paleokarstification and reservoir distribution in the middle triassic carbonates of the member IV of the Leikoupo Formation, northeastern Sichuan Basin. *Acta Petrol. Sin.* 27, 2272–2280.

Zong, K., Klemd, R., Yuan, Y., He, Z., Guo, J., Shi, X., et al. (2017). The assembly of Rodinia: The correlation of early Neoproterozoic (ca. 900 Ma) high-grade metamorphism and continental arc formation in the southern Beishan Orogen, southern Central Asian Orogenic Belt (CAOB). *Precambrian Res.* 290, 32–48. doi:10.1016/j.precamres.2016.12.010

Zou, C., Du, J., and Xu, C. (2014). Formation, distribution, resource potential and discovery of the Sinian-Cambrian giant gas field, Sichuan Basin, SW China. *Petroleum Explor. Dev.* 41 (3), 278–293. doi:10.11698/PED.2014.03.03